The Effect of Triple Particle Sizes on the Mechanical Behaviour of Granular Materials using Discrete Element Method (DEM)

Muath S. Talafha
PhD student
Hungarian University of agriculture and life science
mechanical engineering doctoral school
Hungary

István Oldal
Professor
Hungarian University of agriculture and life science
mechanical engineering doctoral school
Hungary

Granules are used in various industries such as medicine and agriculture, and their behavior is influenced by the characteristics of the constituent particles. The Discrete Element Method (DEM) is a technique for characterizing the mechanical behavior of granular materials by building a mechanical model that describes the impacted parameters, including particle shape, which is being one of these parameters. As a result, the discrete element method is applied to investigate the macro-and micro-mechanical shear behavior of granular materials. For this study, a gravitational disposition for geometrical arrangement model has been used to model various triple particle sizes for a direct shear test using (EDEM®), which is a three-dimensional (3D) program based on (DEM). Different triple particle sizes were used to create an assembly. The results revealed that the size index affected the relationship between shear strength, angular velocity, dilation, coordination number (CN), and volumetric strain.

Keywords: *Discrete element methods, Direct shear test, granular materials, Triple Particle shape*

1. INTRODUCTION

Granular materials have an important role in the medical and agriculture industries. The mechanical behavior of the granular material layer is generally influenced by the loading properties [1], distribution of particle size [2], the void ratio [3], fouling level [4], particles contact [5], and normal stress and confining pressure [6], as well as the properties of individual particles, such as particle size [7], and strength [8], particle shape [9].

The angularity and shape of the surface of the particles influence the behavior of granular materials [10]. It showed that the degradation of the particles is dependent on their form [11]. The flaky or elongated particles tend to break down rather than the cubic. However, in experimental work, it is difficult to provide a straightforward approach to conceptualize the evolution of particle angularity or surface texture. Furthermore, computer simulations are often used in granular materials research due to the high expense of experiments and the restrictions of huge equipment for undertaking large-scale studies.

Due to its discreet complexity, in recent decades, numerical models based on the discrete element method (DEM) have been created to study granular material behavior. Furthermore, DEM allows us to compare the outcomes achieved by varying the properties of the simulated materials, primarily shape indexes [12]. Shear strength, dilatation, and residual shear strength increased significantly as particle angularity increased according to a 2D simulation [13]. Despite this, describing the true geometry of such particles in DEM simulations remains difficult. An early DEM approach could only model a realistic particle type as a disk or spherical particle in 2D and 3D simulations [14]. Despite a simple approach for detecting interactions and measuring forces, the actual particle form should be simulated because the rotation resistance of a disk or sphere is generally lower than the rotation resistance of the actual particle shape. In disks or spheres, rotation is only impacted by tangential contact forces, and the moment on such particles has no effect because the normal force is directed toward the center [15]. Some of these strategies have been used to model ballast particle forms in railway studies.

A ballast settlement was predicted using DEM on polygon-shaped particles, To simulate the actual shape of ballast particles under cyclic stress [16]. Researchers observed that particles smaller than half the nominal maximum size are inappropriate in full-scale ballast layers as a model when modeling ballasts [17]. A similar approach was used [18], while clusters of bound circular particles were used to create a 2D projection of angular ballast particles [19]. Ballast has been modeled similarly using 3D simulations [20].

On the other hand, ellipsoids particles shape [15], an elliptical particle shape and oval-shaped boundary particles [21], polygon-shaped particles [22], dense clusters overlapping particles [23], and particles with an axis symmetry [24], The true shapes of these particles may not be accurately described. In addition, some of these methods need a large amount of computational time. Therefore, to simulate the particle form, an approach has been presented based on a basic algorithm

Received: September 2021, Accepted: November 2021
Correspondence to: Muath S. Talafha
Hungarian University of agriculture and life science,
Gödöllö, H-2103, Pest, Hungary
E-mail: Muath.Sultan.Ahmat.Talafha@hallgato.uni-szie.hu
doi: 10.5937/fme2201139T

that is widely used in DEM [25]. In this procedure, the overlapping spherical pieces are tightly joined. It can describe a particle form with varying angularities while keeping the same contact rules as a single sphere. This technique was applied in several kinds of research to model the actual shape of ballasts. The researchers simulated geogrid-reinforced ballasts To determine the ideal location for a geogrid [26]. In addition, the shear strength decreased with a decrease in the particle friction due to a greater degree of fouling, found that after carrying out a direct test of the shear box [27]. They also discovered that large amounts of fouling cause the fouled ballast samples to dilate, particularly at low normal stress levels. Researchers further stated considerable agreement between lab results and the DEM simulation for coal-filled geogrid stabilized ballasts [28]. Finally, fouling in the ballast bed reduces the sleeper's lateral resistance [29], especially when the fouling material is located in the ballast sheet's shoulder. While most numerical studies have focused on simulating real particle shapes or the mechanical responses of the ballast layer under different conditions, the effects of shape properties on mechanical results, which are difficult to analyze in laboratory experiments, are rarely reported in detail.

In this work, DEM performed a 3D simulation of the direct shear cylinder test. It was done to determine the effect of triple particle shape attributes on the shear strength parameters of the granular layer. The size of the various triple particles was modeled for the numerical simulation. The impacts of shape properties on the behavior of the granular layer for different triple particle size indexes (SI), where the size index defines the relative particle size ratio, triple particles size are investigated using varied levels of normal stresses. Moreover, the effects of a particle shape index on the shear strength of a granular layer and macroscopic response were tested using microscopic measures.

2. THE DISCRETE ELEMENT METHOD (DEM)

Instead of the conventional cost-effective trial-and-error method, the DEM is an excellent tool for modeling the mechanical properties of bulk material and a full process of particle blending [30].

The Discrete Element Method (DEM) was developed to model the mechanical behavior of granular materials by applying the equation of motion to each particle in the material assembly [31]. During the simulation circle, The normal and tangential forces generated by particle-particle and particle–wall interactions are calculated using a cycle that involves applying Newtonian equations of motion repeatedly to generate each particle's acceleration, velocity, and displacement values, as shown below.

$$F_n = \frac{4}{3} E_0 \delta^{\frac{3}{2}} \sqrt{R_0} - 2\sqrt{\frac{5}{6}} \frac{\ln C_r}{\sqrt{\ln^2 C_r + \pi^2}} \sqrt{2E_0} \sqrt[4]{R_0 \delta} \sqrt{m_0 v_{nrel}} \quad (1)$$

The young E_0 module equivalent of two intermingling particles is derived from the following formula.

$1/E_0 = \left(1-\nu^2/E_1 + \left(1-\nu_2^2\right)\right)/E_2 \cdot \delta$ Represents the amount when those two particles collide, and *C*r is the coefficient of restitution (described in EDEM® [32] as the ratio of separation to approach speed in a collision). The normal overlap δ characterizes normal particle deformation.

$$F_t = -8G_0 \sqrt{R_0 \delta \delta_t} - 2\sqrt{\frac{5}{6}} \frac{\ln C_r}{\sqrt{\ln^2 C_r + \pi^2}} \sqrt{2G} \sqrt[4]{R_0 \delta} \sqrt{m_0 v_{trel}} \quad (1)$$

The equivalent shear modulus of two entangled particles G_0 is calculated using the following formula: $1/E_0 = \left(1-\nu^2/E_1 + \left(1-\nu_2^2\right)\right)/E_2 \cdot \delta$ Describes the tangential overlap of two particles, which represents the tangential deformation. And v_{iral} is the tangential component of relative particle velocity. Tangent overlap is the tangential movement between two particles from first to last contact, whether when one particle rolls or slips against another.

The newly discovered displacement is utilized to calculate the contact forces and torques on that location due to the particles' interactions in the new position. This technique is done several times to imitate the bulk material's mechanical behavior [33]. This method is ideal for examining the unique behavior of granular materials and their movement [34] or examining the vibration effect [33]. Researchers proved that their validated model of the discrete element is useful for determining the velocity distribution in a mixed flow dryer and may optimize the dryer geometry [34]. And the researchers have predicted that discrete models might be used to determine and analyze the exact pressure distribution in a silo by simplifying the design process for this sort of equipment [35]. DEM can also investigate flow patterns, segregation, discharge rates, and the effect of flow correction inserts in silos [33]. As can be seen, the discrete element technique is useful in a variety of situations. Contact forces and moments are calculated using DEM based on particle displacement in each time step. The behavior of particles and interactions depends on the geometry and micromechanical properties of particles [33]. EDEM® discrete element software was used with the optimal contact model "Hertz Mindlin No-Slip [32]."

3. DESCRIPTION OF THE NUMERICAL SHEAR CYLINDER

As indicated in Figure 1, the test was conducted in a 225 mm high and a 52 mm radius in a cylindrical system. The bottom cylinder was 75 mm in height and could move freely under the fixed upper cylinder 150 mm in length. The horizontal displacement of the test system was represented by a distance of about 30mm (i.e., around 15% shear strain), which is excellent for recording peak shear stress in particle samples. The vertical loading method can be used to keep the model under constant normal load. Furthermore, a horizontal loading device can deliver a shearing force on the sample at a steady displacement rate in a direction parallel to the lower cylinder movement. For the

particles model, three different triple particles were generated, each triple particle consists of three symmetric spheres, for the first origin particle SI=100%, the radius of the spheres is 1mm where the distance between the spheres' centers is 1.7mm, the second particle SI=125% is larger than the origin particle by 25% therefore, the radius of the spheres is 1.25mm with aspheres center distance is 2.215mm, and the third particle SI=150% is larger than the origin particle by 50% therefore, the sphere's radius is 1.5mm and the sphere's center distance is 2.55 mm as shown in Figure 2. The sphericity index (SPH) remains constant for all simulation repetitions at (SPH= 74%) because the particle size increases the three-dimensional axis. The sphericity index (SPH) is defined as the ratio of particle volume to the smallest circumscribing sphere [36]. The SI has been used to analyze the shapes of the various particles quantitatively.

Several assembly series were performed, three of them (SI= 100%, 125%, 150%) under the normal pressure of 4 kPa and the same under 8 kPa to examine the changing of the normal load and the SI on the mechanical properties of the model. A certain number of particles of the same shape and size were generated for each repetition. The SI=100% assemblies have 55000 particles, SI=125% groups have 28000 particles, and SI=150% groups have 16000 particles. Normal gravity forces compacted the particles that fill the shear cylinder for all samples to allow a successful sample comparison.

Three stages of simulated testing were carried out. Because the program produced particles that contacted neighboring particles and kept kinetic energy, the assemblies produced during the first stage were incredibly fast. As a result, the particles took some time to settle down and reach zero kinetic energy. During the second phase of assembly, the needed vertical load has been applied. Using almost the same shear system diameter particles with the correctly calculated density enables a suitable vertical load. The vertical load's spherical shape assists in avoiding load weight tilting, which is a common issue during DEM shear tests [37]. The third step was to run a direct shear test, which involved shifting the lower cylinder of the shear system horizontally while maintaining a constant vertical load throughout shearing. As Figure 3 illustrates.

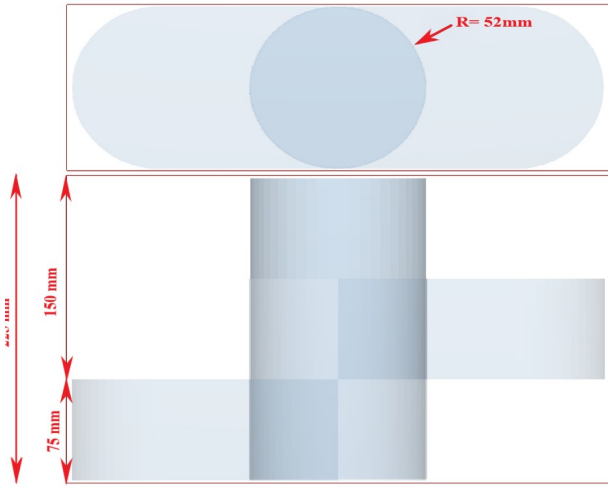

Figure 1. Schematic of Shear cylinder geometry

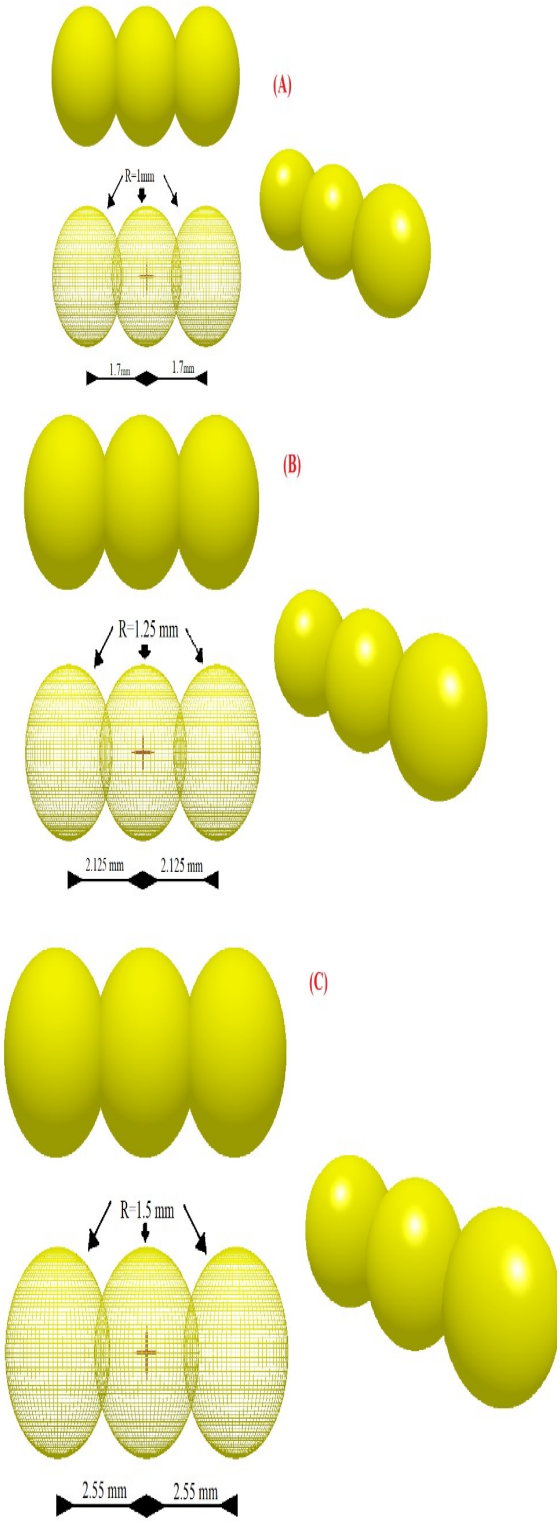

Figure 2 Various particle SI simulations (SI= 100%, 125%, 150% for all the particles, respectively).

Table 1 Micromechanical parameters of the model.

Parameter	Value
Particles Poisson's ratio	0.25
Wall Poisson's ratio	0.3
Particles Shear modulus (Pa)	1×10^8
Wall Shear modulus (Pa)	8×10^10
Coefficient of restitution	0.5
Coefficient of rolling friction	0.01
Particle density (kg/m3)	2500
Coefficient of interparticle friction	0.5
Coefficient of plane wall-particle friction	0.5

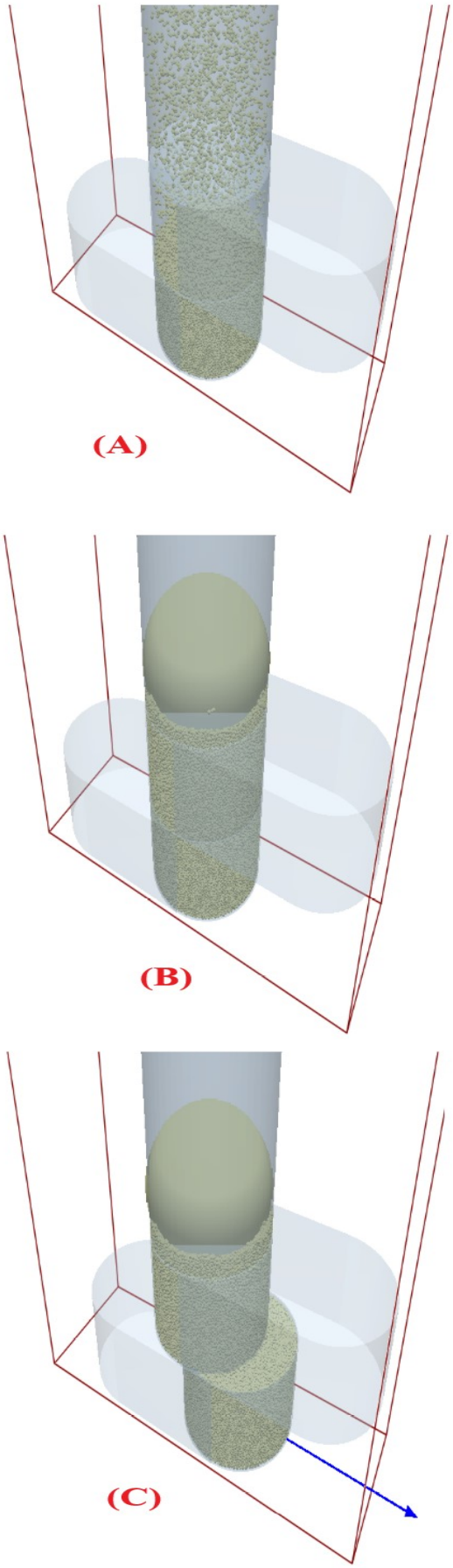

Figure 3 Simulation of Shear cylinder and the Stages of assembled generation particles with a size ratio of 100% under the normal pressure of 8 kPa. (A Initially generated, B compacted and applied normal stress, C finally sheared)

Table 1 shows the used Micromechanical properties of the DEM model based on previous work of [38][39].

4. SIMULATION RESULTS AND DISCUSSION

In terms of particle size properties, this section covers the macroscopic and microscopic findings for the direct shear behavior of DEM numerical simulations for various triple particle samples. Shear stress, volumetric strain, a network of contact forces, contact number variance, and average particle rotation within the cylinders are some of the findings.

4.1 Shear stress

Under constant normal stresses, the relationship between shear stress and horizontal strain for particle samples with varied size indexes is shown in the figure below. The internal friction angle was calculated by using the arctangent of the shearing stress ratio to the normal stress (φ = arcing ($\tau.\sigma$)). The internal friction angle was shown to be positively related to particle size. The particle size impacts the internal friction angle. When the particle size is at its maximum, the peak friction angle first tends to approach a higher limit; growing particle size is crucial, and its effect is considerable. For 2D elliptical particles, similar results were achieved [15], and it has identical findings For 3D ellipsoid, multi-sphere assemblies [40].

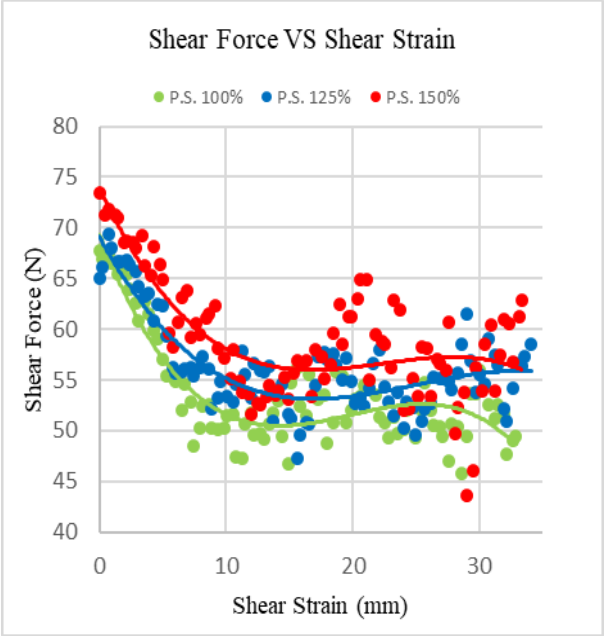

Figure 4 Shear force with shear displacement curves of samples with various SI at a normal stress of 8 kPa

The influence of SI is more visible on particle specimens, as illustrated in (Figure 4), which shows the size index's reflection on particle shear force. This phenomenon is represented by the growth of the moment force and the course interlocking connections between particles under normal stress (course interaction between particles). The large particles would be more frictionally interlocked due to an increase in normal load, which led to the rise in the critical moment to rotate the particle. For example, when the particle's SI

changed from 100% to 150% at 8 kPa normal stress, the shear force increases about 13% from 51N to 58N. However, for small size index particles, the change in shear force was decreased, and vice versa.

4.2 Volumetric strain

Figure 5 compares volumetric strain variations with horizontal strain for various SI under constant normal loads. The overall volumetric strain increases as the SI increases, indicating that dilatancy in bigger particles increases as the SI increases. Demonstrating that dilatancy is affected by particle shape and normal load [37].

The dilation values for (SI=150%) assembly is 57% larger than the (SI= 100%) assembly at a normal stress of 8 kPa.

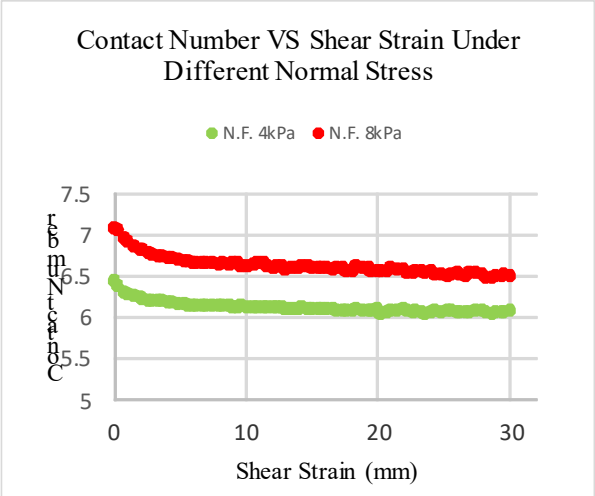

Figure 5 Variations of volumetric strain with shear strain for different size index at normal pressure of 8 kPa.

4.3 Average contact numbers

The coordination number (CN) is calculated by averaging the number of particles in contact with the total number of particles in the assembly. Because particle interaction is connected to points of contact, CN is a relevant parameter to explain the behavior of granular materials [41].

As SI increases, CN is found to be constant. When the SI changes, the CN remains relatively constant, as demonstrated in (Figure 6). which can be explained. The changes do not interfere with the particle's sphericity; because the particle shape was maintained. As a result, the density of the particle connections in the assembly remained relatively unchanged. Therefore, the sphericity index will remain constant. Researchers mentioned that when the SPH index is changed, the particle shape changes in one dimension, causing the particle to become more elongated, increasing the interlocking between the particles and allowing other particles to contact the same particle, resulting in an increase in the CN [37].

When the sample was subjected to high pressure, a bigger CN was formed regardless of the SI index, as shown in (Figure 7). On the other hand, the initial shear stress generates an immediate drop in the CN at lower normal stress due to greater dilatation.

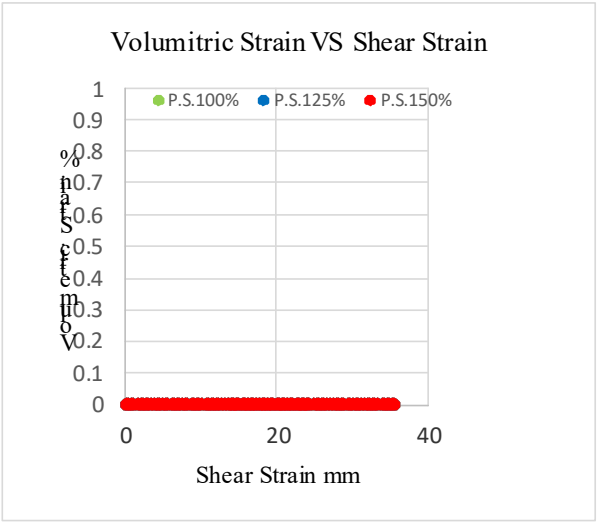

Figure 6 Variations of CN versus shear strain for normal stress of 8 kPa (SI effect).

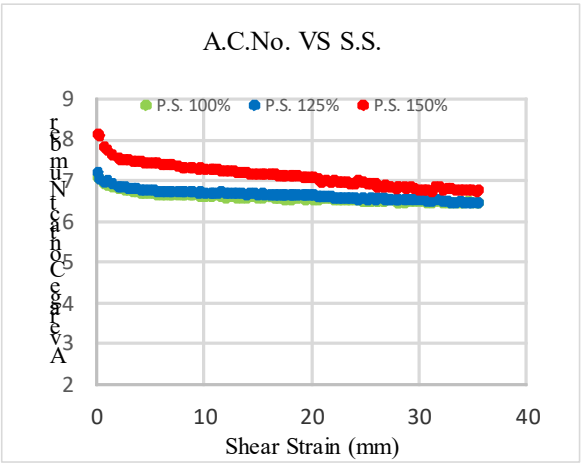

Figure 7 Variations of CN versus shear strain with various normal stresses 4kPa and 8kPa for a sample of (SI= 100%).

4.4 Contact force chain

(Figures 8 and 9) demonstrate the distributions of inter-particle and particle-wall forces for various SI values under constant normal stress at different stages of the direct shear test. The colors of the particles in (Figures 8 and 9) are proportional to the strength of the contact forces in the assembly, with red, green, and blue particles representing strong, moderate, and low forces, respectively. The contact forces in the shear container are evenly distributed independently of particle shape previous to shear loading (at a strain of 0%). Contact force chains vary dramatically as shear force is applied, with a strain of 15% compared to a strain of 0% during shearing. The first step (Figure 8) exhibits a larger chain than the shear stage (Figure 9). Due to the dilatation of particles during shearing, which reduces the number of interactions. The shear stage illustrates the number of contacts directed toward high loads (i.e. the direction of shear) and a reduction in shear forces resulting from the decrease in the contact area. It's also been discovered that samples with a higher SI have a larger shear force in the shear stage. As a result of enhanced rough interlocking, assemblies with higher SI values showed greater observed strength. The higher SI samples revealed a force concentration around the top shear

cylinder's vertical walls. These findings are comparable to [42], who stated that strong force chains formed a greater portion of the assembly contacts in higher granular samples. This rearrangement causes the shear band to shape entirely from the top right to the bottom left of the shear cylinder, providing a good load transmission in the samples. As a result, the structure from which force chains are formed is more stable, while on the other hand, the particles located outside of the shear band are not involved in carrying the load.

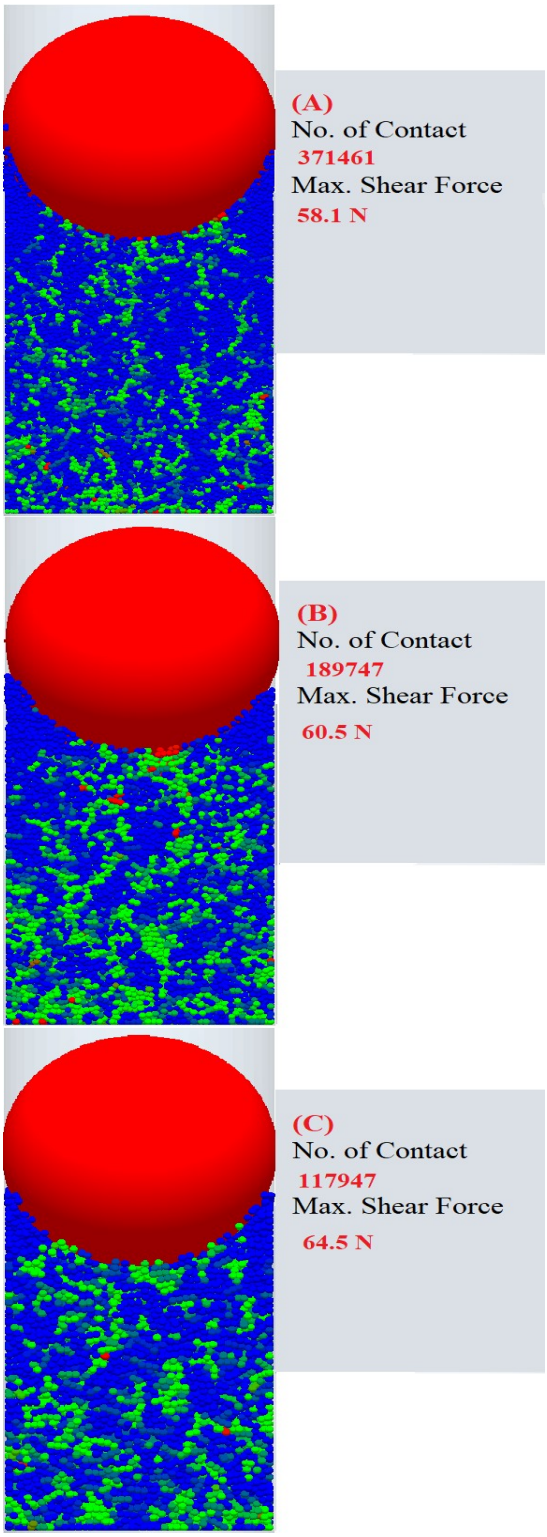

Figure 8 Contact force chain distribution for different size index particles at shear strain of 0% and 8kPa normal stress (Size index SI= 100%, 125%, 150% respectively).

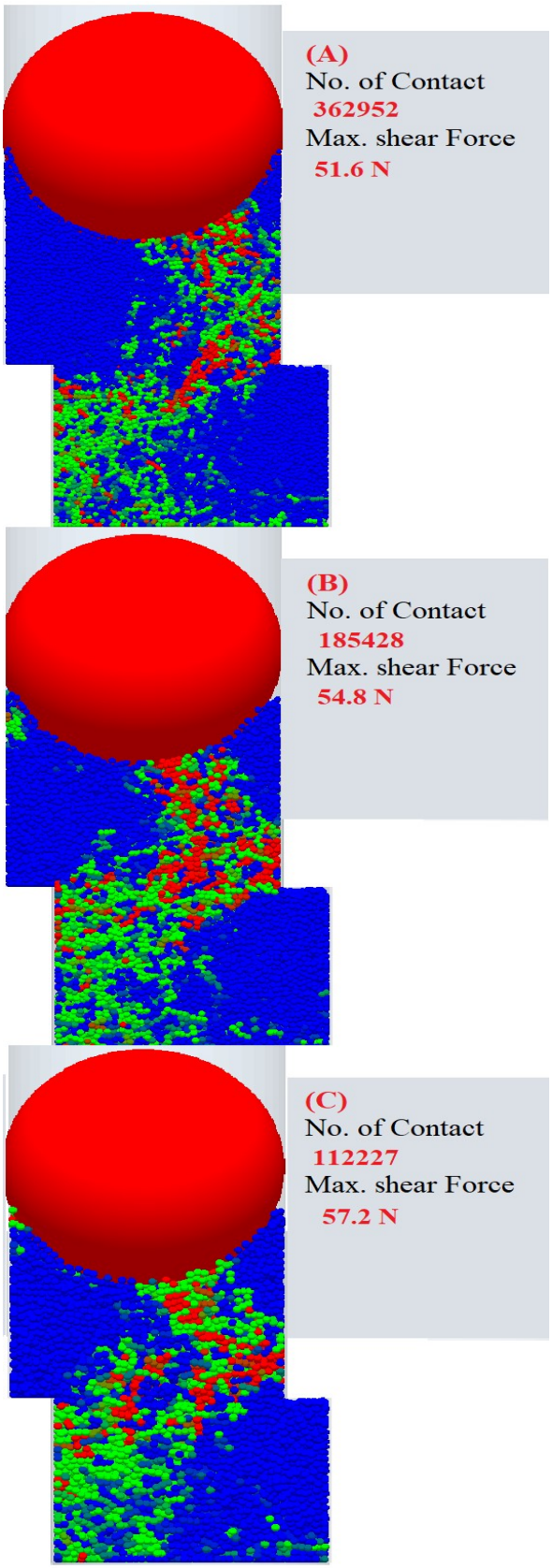

Figure 9 Contact force chain distribution for different size index particles at shear strain of 15% and 8kPa normal stress (Size index SI= 100%, 125%, 150% respectively).

4.5 particle rotation

Particle rotation is a simple method for assessing the formation of shear bands in granular assemblies during loading [43]. While the shear band can be evaluated in a

direct shear test, the effect of the particle SI must be further analyzed in terms of the position of the shear band and the average angular velocity, where it has been considered the average angular velocity in this paper. Therefore, (Figures 10&11) are plotted. The average angular velocity is observed for both small and large particles. The average accumulation rotation is lower for large particles SI=150% than for small particles SI=100%. As shown in Figures (10&11), the interlocking between the particles increases as the SI increases, and the average rotation of the particle decreases. For example, changing the particle shape from SI=100% to SI=150% reduces the average particle rotation by 24%. Additionally, The increase in shear strength caused by an increase in the SI is accompanied by a decrease in the particle's average rotation [41].

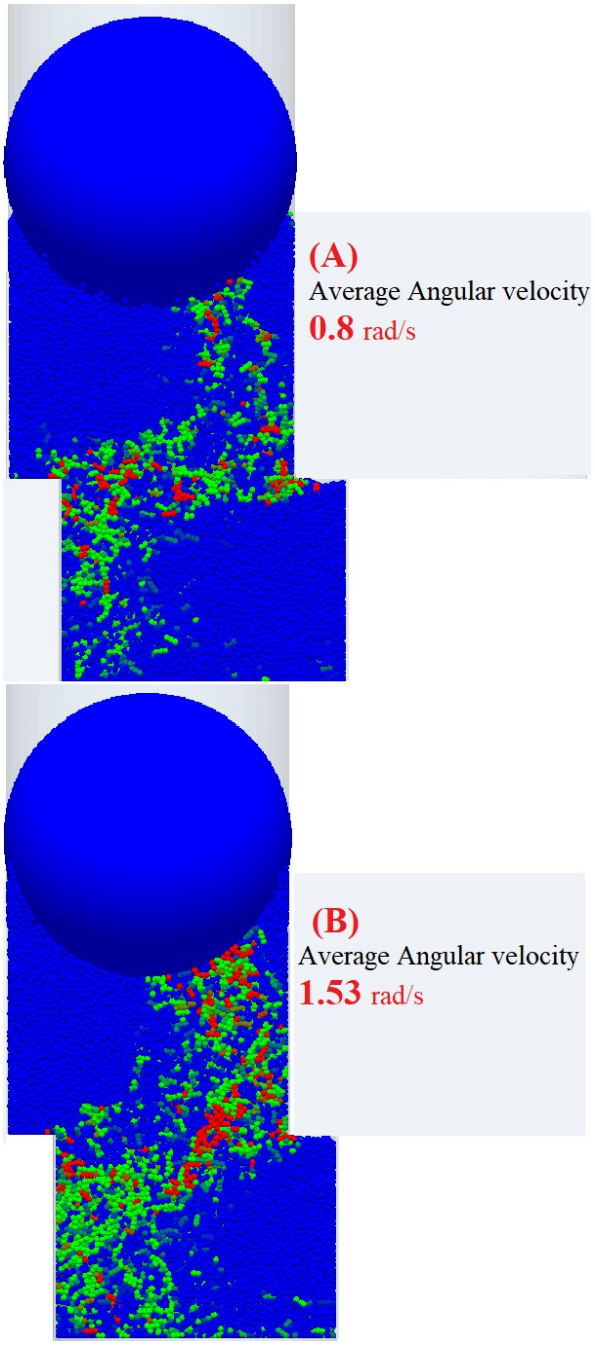

Figure 10 Average angular velocity for different size index particles under 8kPa normal stress.

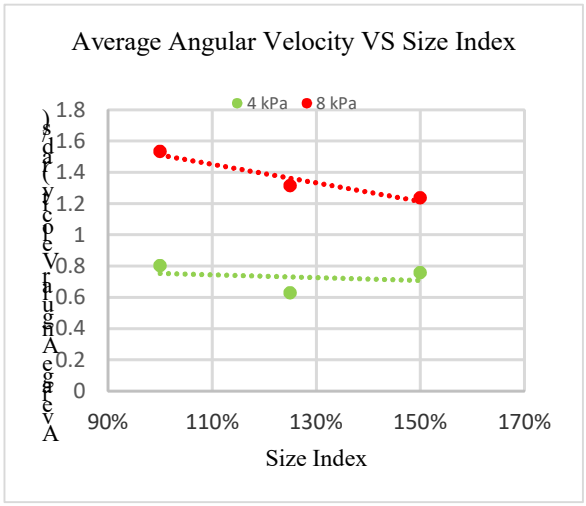

Figure 11 Average angular velocity for different size indexes at a normal stress of 4 and 8 kPa.

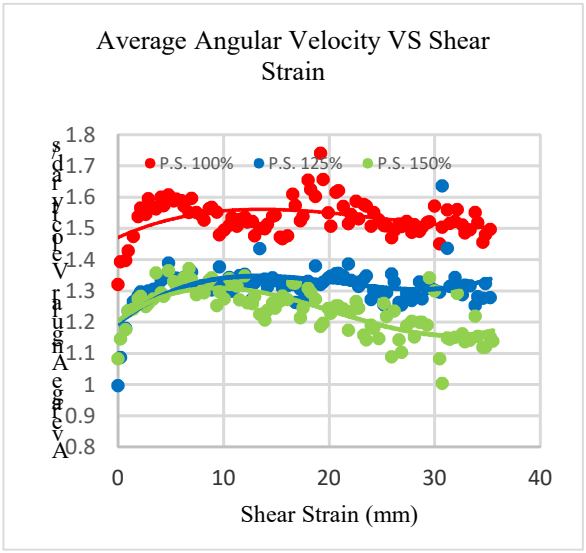

Figure 12 Particle rotation at a shear strain of 15% for a test of SI 100% at a different normal stress of 4 kPa, 8 kPa, respectively.

The particles movement behavior can be described as a layer's movement on top of each other, as shown in (Figure 12). The normal force influences the rotation relationship in the particles due to better interlocking between the particles, which in the end, will increase the friction between the particles. Therefore, the rotation of the particles will increase due to better as shown in (Figure 11). The pattern of the rotation of the particles follows the distribution of the load band particles, as shown previously in (Figures 9).

5. CONCLUSION

In this research, the influence of triple particle shape properties on particles layer behavior was numerically investigated. A 3D DEM software was used to create the actual shape of the particles for the direct shear cylinder test. Three assemblies were made and tested under various normal stresses with varying size indexes. These particle shape indexes are within an acceptable range.

The following are the key findings from the examination of both macro-and micro-mechanical responses:

1. Regardless of particle shape, dilation decreases with increasing normal stress in all samples.

2. The SI (size index) increases dilation, but as normal stress increases, the effect of this increase becomes insignificant.

3. Initially, shear strength, and dilation, decrease with a decrease in SI values.

4. Size index does not affect the coordination number (CN) value, and the (CN) is consistent with the dilation behavior of the assemblies. A reduction in CN accompanies increased dilation.

5. The particles' movement behavior can be explained as a movement of layers on top of each other.

6. In the initial stage of shearing, the distributions of the inter-particle force are distributed equally in all assemblies, then the number of contacts oriented in directions with higher stress and their magnitude inc–releases.

7. For small-sized particles, the average particle rotation is higher than big-sized particles due to less particle dilation.

In general, size index variation has a significant individual effect on ballast sample shear strength.

ACKNOWLEDGEMENT

This work was supported by the Stipendium Hungaricum Program and by the Mechanical Engineering Doctoral School, The Hungarian University of Agriculture and Life Sciences, Gödöllő, Hungary.

REFERENCES

[1] A. S. J. Suiker, E. T. Selig, R. Frenkel, "Static and cyclic triaxial testing of ballast and sub-ballast," *J. Geotech. Geoenvironmental Eng.*, vol. 131, no. 6, pp. 771–782, Jun. 2005, doi: 10.1061/(ASCE) 1090-0241(2005) 131:6 (771).

[2] B. Indraratna, H. Khabbaz, W. Salim, and D. Christie, "Geotechnical properties of ballast and the role of geosynthetics in rail track stabilization," *Proc. Inst. Civ. Eng. - Gr. Improv.*, vol. 10, no. 3, pp. 91–101, Jul. 2006, doi: 10.1680/grim.2006. 10.3.91.

[3] G. P. Raymond and J. R. Davies, "TRIAXIAL TESTS ON DOLOMITE RAILROAD BALLAST," *ASCE J Geotech Eng Div*, vol. 104, no. 6, pp. 737–751, 1978, doi: 10.1016/0148-9062(78)91498-5.

[4] H. Huang, E. Tutumluer, and W. Dombrow, "Laboratory Characterization of Fouled Railroad Ballast Behavior," *Transp. Res. Rec. J. Transp. Res. Board*, vol. 2117, no. 1, pp. 93–101, Jan. 2009, doi: 10.3141/2117-12.

[5] A. Haber, G. K.-F. Transactions, and undefined 2020, "Development of a new DEM contact model for hygroscopic bulk solids," *scindeks.ceon.rs*, doi: 10.5937/fme2002432H.

[6] J. Lackenby, B. Indraratna, G. McDowell, and D. Christie, "Effect of confining pressure on ballast degradation and deformation under cyclic triaxial loading," *Géotechnique*, vol. 57, no. 6, pp. 527–536, Aug. 2007, doi: 10.1680 /geot.2007.57.6.527.

[7] W. L. Lim, G. R. Mcdowell, and A. C. Collop, "The application of Weibull statistics to the strength of railway ballast," *Granul. Matter*, vol. 6, pp. 229–237, 2004, doi: 10.1007/s10035-004-0180-z.

[8] M. Koohmishi and M. Palassi, "Evaluation of the Strength of Railway Ballast Using Point Load Test for Various Size Fractions and Particle Shapes," *Rock Mech. Rock Eng.*, vol. 49, no. 7, pp. 2655–2664, Jul. 2016, doi: 10.1007/s00603-016-0914-3.

[9] E. Tutumluer and Y. M. A. Hashash, "Aggregate Shape Effects on Ballast Tamping and Railroad Track Lateral Stability.," Sep. 2006. Accessed: Jul. 22, 2020. [Online]. Available: https://www.researchgate.net/publication/237116793.

[10] D. Li, J. Hyslip, T. Sussmann, and S. Chrismer, *Railway geotechnics*. 2015.

[11] Y. Guo, V. Markine, J. Song, and G. Jing, "Ballast degradation: Effect of particle size and shape using Los Angeles Abrasion test and image analysis," *Constr. Build. Mater.*, vol. 169, pp. 414–424, Apr. 2018, doi: 10.1016/j.conbuildmat.2018.02.170.

[12] S. Lobo-Guerrero and L. E. Vallejo, "Discrete element method analysis of rail track ballast degradation during cyclic loading," *Granul. Matter*, vol. 8, no. 3–4, pp. 195–204, 2006, doi: 10.1007/s10035-006-0006-2.

[13] S. Abedi, A. A. Mirghasemi, "Particle shape consideration in numerical simulation of assemblies of irregularly shaped particles," *Particuology*, vol. 9, no. 4, pp. 387–397, Aug. 2011, doi: 10.1016/j.partic.2010.11.005.

[14] P. A. Cundall and O. D. L. Strack, "A discrete numerical model for granular assemblies," *Géotechnique*, vol. 29, no. 1, pp. 47–65, Mar. 1979, doi: 10.1680/geot.1979.29.1.47.

[15] L. Rothenburg and R. J. Bathurst, "Micromechanical features of granular assemblies with planar elliptical particles," *Geotechnique*, vol. 42, no. 1, pp. 79–95, Mar. 1992, doi: 10.1680/geot.1992.42.1.79.

[16] E. Tutumluer, Y. Qian, Y. M. A. Hashash, J. Ghaboussi, and D. D. Davis, "Discrete element modelling of ballasted track deformation behavior," *Int. J. Rail Transp.*, vol. 1, no. 1–2, pp. 57–73, Feb. 2013, doi: 10.1080/23248378 .2013.788361.

[17] [X. Bian, H. Huang, E. Tutumluer, and Y. Gao, "'Critical particle size' and ballast gradation studied by Discrete Element Modeling," *Transp. Geotech.*, vol. 6, pp. 38–44, Mar. 2016, doi: 10.1016/j.trgeo.2016.01.002.

[18] G. Saussine *et al.*, "Modelling ballast behavior under dynamic loading. Part 1: A 2D polygonal discrete element method approach," *Comput. Methods Appl. Mech. Eng.*, vol. 195, pp. 2841–2859, 2006, doi: 10.1016/j.cma.2005 .07.006ï.

[19] B. Indraratna, P. K. Thakur, and J. S. Vinod, "Experimental and Numerical Study of Railway

Ballast Behavior under Cyclic Loading," *Int. J. Geomech.*, vol. 10, no. 4, pp. 136–144, Aug. 2010, doi: 10.1061/(ASCE) GM.1943-5622.0000055.

[20] G. Jing, K. Feng, L. Gao, and J. Wang, "DEM simulation of ballast degradation and breakage under cyclic loading," *Xinan Jiaotong Daxue Xuebao/Journal Southwest Jiaotong Univ.*, vol. 47, no. 2, pp. 187–191, 2012, doi:10.3969 /j.issn.0258-2724.2012.02.003.

[21] A. V. Potapov, C. S. Campbell, "A fast model for the simulation of non-round particles," *Granul. Matter*, vol. 1, no. 1, pp. 9–14, 1998, doi: 10.1007/PL00010910.

[22] A. A. Mirghasemi, L. Rothenburg, and E. L. Matyas, "Numerical simulations of assemblies of two-dimensional polygon-shaped particles and effects of confining pressure on shear strength," *Soils Found.*, vol. 37, no. 3, pp. 43–52, Sep. 1997, doi: 10.3208/sandf.37.3_43.

[23] J. F. Favier, M. H. Abbaspour-Fard, and M. Kremmer, "Modeling Nonspherical Particles Using Multisphere Discrete Elements," *J. Eng. Mech.*, vol. 127, no. 10, pp. 971–977, Oct. 2001, doi: 10.1061/(ASCE)0733-9399(2001) 127:10(971).

[24] R. P. Jensen, P. J. Bosscher, M. E. Plesha, T. B. Edil, "DEM simulation of granular media-structure interface: effects of surface roughness and particle shape," *Int. J. Numer. Anal. Methods Geomech.*, vol. 23, no. 6, pp. 531–547, May 1999, doi: 10.1002/(SICI)1096-9853 (199 905)23:6<531::AID-NAG980>3.0.CO;2-V.

[25] T. Matsushima, H. Saomoto, "Discrete element modeling for irregularly-shaped sand grains," *Proc. NUMGE2002 Numer. Methods Geotech. Eng.*, no. May, pp. 239–246, 2002, Accessed: Jul. 22, 2020. [Online]. Available: https:// pascal-francis.inist.fr/vibad/index.php?action= getRecordDetail&idt=16398173.

[26] C. Chen, G. R. McDowell, and N. H. Thom, "Discrete element modelling of cyclic loads of geogrid-reinforced ballast under confined and unconfined conditions," *Geotext. Geomem–branes*, vol. 35, pp. 76–86, Dec. 2012, doi: 10.1016/j.geotexmem.2012.07.004.

[27] B. Indraratna, N. T. Ngo, C. Rujikiatkamjorn, and J. S. Vinod, "Behavior of fresh and fouled railway ballast subjected to direct shear testing: Discrete element simulation," *Int. J. Geomech.*, vol. 14, no. 1, pp. 34–44, Feb. 2014, doi: 10.1061/(ASCE)GM.1943-5622.0000264.

[28] N. T. Ngo, B. Indraratna, C. Rujikiatkamjorn, "DEM simulation of the behaviour of geogrid stabilized ballast fouled with coal," *Comput. Geotech.*, vol. 55, pp. 224–231, Jan. 2014, doi: 10.1016/j.compgeo.2013.09.008.

[29] H. Xu and S. J. Liao, "Laminar flow and heat transfer in the boundary-layer of non-Newtonian fluids over a stretching flat sheet," *Comput. Math. with Appl.*, vol. 57, no. 9, pp. 1425–1431, 2009, doi: 10.1016/j.camwa.2009 .01.029.

[30] S. Garneoui, "Mixing Enhancement of Wheat Granules in a Hopper Bottom Lab-Scale Mixer Using Discrete Element Simulations," pp. 868–873, 2020, doi: 10.5937/fme2004868G.

[31] P. A. Cundall and O. D. L. Strack, "Cundall _Strack.Pdf." pp. 47–65, 1979.

[32] "DEM Solution. EDEM 2.7.0 User Guide. Edinburgh, United... - Google Scholar." https:// scholar.google.com/scholar?q=DEM Solution. EDEM 2.7.0 User Guide. Edinburgh%2C United Kingdom %282015%29 (accessed Nov. 26, 2021).

[33] I. Oldal, F. Safranyik, "Extension of silo discharge model based on discrete element method," *J. Mech. Sci. Technol.*, vol. 29, no. 9, pp. 3789–3796, Sep. 2015, doi: 10.1007/s12 206-015-0825-3.

[34] I. Keppler, L. Kocsis, I. Oldal, I. Farkas, and A. Csatar, "Grain velocity distribution in a mixed flow dryer," *Adv. Powder Technol.*, vol. 23, no. 6, pp. 824–832, Nov. 2012, doi: 10. 1016/j.apt.2011.11.003.

[35] C. González-Montellano, A. Ramírez, J. M. Fuentes, F. Ayuga, "Numerical effects derived from en masse filling of agricultural silos in DEM simulations," *Comput. Electron. Agric.*, vol. 81, pp. 113–123, 2012, doi: 10.1016/ j.compag.2011.11.013.

[36] W. C. Krumbein, "Measurement and Geological Significance of Shape and Roundness of Sedimentary Particles," *SEPM J. Sediment. Res.*, vol. Vol. 11, no. 2, pp. 64–72, Aug. 1941, doi: 10.1306/d42690f3-2b26-11d7-864800010 2c1865d.

[37] M. S. Talafha, I. Oldal, "Evaluation the effect of particle sphericity on direct shear mechanical behavior of granular materials using discrete element method (DEM)," *Int. J. Eng. Model.*, vol. 34, no. 1, pp. 1–18, Feb. 2021, doi: 10.31534/engmod.2021.1.ri.01m.

[38] I. Oldal and F. Safranyik, "Extension of silo discharge model based on discrete element method," *J. Mech. Sci. Technol.*, vol. 29, no. 9, pp. 3789–3796, 2015,doi:10.1007/s12206-015-0825-3.

[39] I. Keppler, et al.: "Grain velocity distribution in a mixed flow dryer," *Adv. Powder Technol.*, vol. 23, no. 6, pp. 824–832, 2012, doi: 10.1016/j.apt.2011.11.003.

[40] J. Gong and J. Liu, "Effect of aspect ratio on triaxial compression of multi-sphere ellipsoid assemblies simulated using a discrete element method," *Particuology*, vol. 32, pp. 49–62, Jun. 2017, doi: 10.1016/j.partic.2016.07.007.

[41] A. Danesh, A. A. Mirghasemi, and M. Palassi, "Evaluation of particle shape on the direct shear mechanical behavior of ballast assembly using discrete element method (DEM)," *Transp. Geotech.*, vol. 23, p. 100357, Jun. 2020, doi: 10.1016/j.trgeo.2020.100357.

[42] Y. Yang, J. F. Wang, and Y. M. Cheng, "Quantified evaluation of particle shape effects from micro-to-macro scales for non-convex

grains," *Particuology*, vol. 25, pp. 23–35, Apr. 2016, doi: 10.1016/j.partic.2015.01.008.

[43] M. Oda, H. Kazama, "Microstructure of shear bands and its relation to the mechanisms of dilatancy and failure of dense granular soils," *Géotechnique*, vol. 48, no. 4, pp. 465–481, Aug. 1998, doi: 10.1680/geot.1998 .48.4.465:

УТИЦАЈ ТРОСТРУКЕ ВЕЛИЧИНЕ ЧЕСТИЦА НА МЕХАНИЧКО ПОНАШАЊЕ ЗРНАСТИХ МАТЕРИЈАЛА ПРИМЕНО МЕТОДЕ ДИСКРЕТНИХ ЕЛЕМЕНАТА (МДЕ)

М.С. Талафа, И. Олдал

Грануле се користе у разним индустријама као што су медицина и пољопривреда, а на њихово понашање утичу карактеристике саставних честица. Метода дискретних елемената (МДЕ) је техника за карактеризацију механичког понашања зрнастих материјала изградњом механичког модела који описује параметре погођене утицајем, укључујући облик честице, који је један од ових параметара.

Као резултат, метода дискретних елемената се примењује за испитивање макро- и микро-механичког понашања зрнастих материјала на смицање. За потребе овог истраживања, грави–тациона диспозиција за модел геометријског уређења је коришћена за моделовање различитих троструких величина честица за директни тест смицања коришћењем (EDEM®), који је тродиментзионални (3Д) програм заснован на (МДЕ). За креирање склопа коришћене су различите троструке величине честица. Резултати су открили да је индекс величине утицао на однос између чврстоће на сми–цање, угаоне брзине, дилатације, координационог броја (ЦН) и волуметријског напрезања.